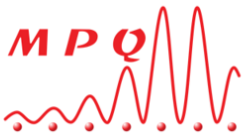

Université Paris Cité
Lab: Matériaux et Phénomènes Quantiques (MPQ)
Group: Dispositifs Optiques Non-linéaires (DON)

Internship Report

M2 - Quantum Devices
Double Degree Program NanoQuad

Z-SCAN SETUP FOR THE OPTICAL CHARACTERIZATION OF COMPLEX $\chi^{(3)}$ OF PLASMONIC METASURFACES.

CANDIDATE
Giorgio GUERCIO

SUPERVISOR
Giuseppe LEO

Paris
June, 2022

Abstract

The main aim of my master internship has been the realization of a Z-scan set-up, for the spectral measurement of the real and imaginary part of the third order nonlinear susceptibility $\chi^{(3)}$ in different materials.

In this report, it will be discussed the theoretical background behind the technique, the optimization steps needed to improve its performances, plus the analysis of different samples, ranging from two different kinds of glasses (a NG11 filter and a microscope glass piece), a polished GaAs sample and some nonlinear colloidal quantum dots clusters provided by Centre de Recherche Paul Pascal.

Contents

List of Tables

List of Figures

Introduction

In recent years, interest in nonlinear optics has steadily increased. This was possible thanks to advancements in various fabrication techniques that allow to create material with some very particular properties. In order to characterize such properties, well established measurement techniques have seen a sudden resurgence; among these, the Z-scan setup allows to measure in a simple, yet effective way the complex $\chi^{(3)}$ of different materials. $\chi^{(3)}$ plays a key role in several nonlinear processes, like the optical Kerr effect, four wave mixing and third harmonic generation.

The main aim of this report is to outline the working principle of such technique while also reporting the possible optimization steps.

In Chapter 1, a quick review of some relevant physical notions is provided, including Gaussian beams, linear and nonlinear optics, with a particular focus on the nonlinear index of refraction and two-photon absorption.

In Chapter 2, an exhaustive overview of the theory behind the Z-scan setup is provided, discussing the two possible cases that can be measured (purely nonlinear refractive materials or materials that also show nonlinear absorption) and the limitations of the setup.

In Chapter 3, I reported the main steps needed to optimize the setup, together with the final setup description and a brief mention of the Knife-edge technique, used to carefully characterize the laser beam.

Finally, in Chapter 4, I reported a series of calibration measurements performed on two different glass types and a GaAs sample.

My internship took place at MPQ (Laboratoire Matériaux et Phénomènes Quantiques), under the DON (Dispositifs Optiques Nonlinéaires). The group research activities lie at the intersection of nanophotonics, nonlinear integrated optics, optomechanics and quantum physics. Combining light and semiconductor nanotechnologies, they aim at the emergence of innovative concepts and devices, at the frontier of scientific and technical knowledge in photonics. In particular, I worked under the supervision of Giuseppe Leo, whose group focuses on the study of optical metasurfaces, nonlinear optics, quantum optics and nanophotonics.

Chapter 1

Theoretical Background

In order to elucidate the working principle of the Z-scan technique, a reminder of some physical notions is needed.
In this chapter, a quick review of the Gaussian beam properties and of the third order non-linearity effects (crucial for the Z-scan operation) will be presented.

1.1 Gaussian beams

A large number of problems in optics can be described by using plane waves, i.e., infinitely extended fields with a constant amplitude and phase in a plane transverse to the propagation direction. However, in nonlinear optics a great deal of phenomena can not always be explained using this approximation. This is particularly true for laser beams, since they have a finite size and vary spatially in the transverse plane. In the theoretical formulation, the transverse profile of a laser is often described by the TEM_{00} mode of a circular Gaussian beam:

$$\tilde{\mathbf{E}}(r,z,t) = \hat{\mathbf{e}} E_0(z,t) \frac{w_0}{w(z)} \exp(-\frac{r^2}{w^2(z)} - \frac{ikr^2}{2R(z)}) e^{-i\phi(z,t)} + c.c. \tag{1.1}$$

where $r = \sqrt{x^2+y^2}$ is the radial coordinate and $E_0(z,t)$ is the on-axis (for $r=0$) amplitude. The Gaussian beam symmetry is illustrated in Fig.1.1.

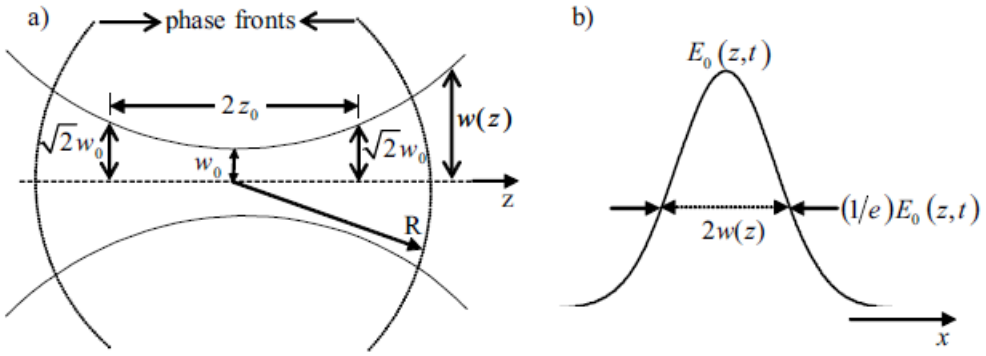

Figure 1.1: Schematic illustration of a TEM_{00} Gaussian beam (a) beam propagation profile. (b) beam cross section.[2]

The beam cross section is described by radius $w(z)$, defined as the half-width of the Gaussian curve at point r, where the curve is at $1/e$ of its maximum value. The radius has a minimum, defined by w_0 (the beam waist), at the plane $z = 0$. Outside this plane, the waist changes with z according to:

$$w(z) = w_0\sqrt{1 + \frac{z^2}{z_0^2}} \tag{1.2}$$

where z_0 is the Rayleigh range, which can also be defined as:

$$z_0 = \frac{2\pi}{\lambda}\frac{w_0^2}{2}. \tag{1.3}$$

The range $|z| < z_0$ is often called near-field of the Gaussian beam while $|z| > z_0$ is called far field. The radius of the curvature of the Gaussian wave-front is given by:

$$R(z) = z(1 + \frac{z_0^2}{z^2}) \tag{1.4}$$

The $e^{-i\phi(z,t)}$ term contains all the radially uniform phase variations. In the near-field region, the phase has practically an infinite radius of curvature and hence the Gaussian beam mimics a plane wave.

1.2 Linear optics

For the majority of situations considered in optics, it can be assumed that the material system is non-magnetic and electrically neutral. Under such assumptions the following wave

equation describes the propagation of light in the medium:

$$\nabla^2\tilde{\mathbf{E}} - \frac{1}{c^2}\frac{\partial^2}{\partial t^2}\tilde{\mathbf{E}} = \frac{1}{\epsilon_0 c^2}\frac{\partial^2}{\partial t^2}\tilde{\mathbf{P}} \tag{1.5}$$

Here, $\tilde{\mathbf{P}}$ denotes the polarization vector which represents the response of the material to the electric field of the electromagnetic wave. Generally, this optical response depends on the field strength and, as a first approximation, $\tilde{\mathbf{P}}$ is linearly related to $\tilde{\mathbf{E}}$:

$$\tilde{P}_i = \epsilon_0 \sum_j \chi_{ij}^{(1)} \tilde{E}_j \tag{1.6}$$

where i, j indicate the Cartesian components of the field and $\chi_{ij}^{(1)}$ are elements of the second-rank tensor of linear susceptibility.

In general, the material does not respond instantaneously to an applied field, losses occur, and $\chi_{ij}^{(1)}$ is both complex and frequency dependent.
In the linear regime, the wave equation in Eq. 1.5 has homogeneous nature. To simplify the problem, the equation is rewritten in terms of the Fourier transform of the electric field, as a time-independent differential equation:

$$\nabla^2\mathbf{E}(\mathbf{r},\omega) - \epsilon_r \frac{\omega^2}{c^2}\mathbf{E}(\mathbf{r},\omega) = 0 \tag{1.7}$$

where, $\epsilon_r = \delta_{ij} + \chi_{ij}^{(1)}$ is the linear dielectric tensor. For simplicity, let us consider a plane wave in an isotropic medium where the linear susceptibility becomes a scalar quantity. The latter is, in general, a complex function of the frequency: $\chi^{(1)}(\omega) = \chi_R^{(1)}(\omega) + i\chi_I^{(1)}(\omega)$. Therefore, the dielectric constant is also complex, but when $\chi_I^{(1)}(\omega) \ll \chi_R^{(1)}(\omega)$ one can write (see Appendix A.1 for derivation):

$$\sqrt{\epsilon_r(\omega)} \approx n_0(\omega) + i\frac{c}{2\omega}\alpha(\omega) \tag{1.8}$$

the real part n_0 is the conventional refractive index while the imaginary part $\kappa = c\alpha/2\omega$ is known as the extinction coefficient. The latter describes the attenuation of the electric field in the medium. The linear refractive index is related to the real part of the linear susceptibility, while the absorption coefficient is proportional to its imaginary part:

$$n_0 = \sqrt{1 + \chi_R^{(1)}} \tag{1.9}$$

$$\alpha = \frac{\omega}{n_0 c}\chi_I^{(1)} \tag{1.10}$$

In these conditions, the plane-wave solution of the linear wave equation in an isotropic medium is:

$$\tilde{\mathbf{E}}(z,t) = \hat{\mathbf{e}}E_0 \exp(-\frac{1}{2}\alpha z)\exp[i(k'z - \omega t)] + c.c. \tag{1.11}$$

where E_0 is the amplitude of the wave at z = 0. The dispersive dependence of the refractive index is included in the wave number: $k' = kn_0(\omega) = n_0(\omega)2\pi/\lambda = n_0(\omega)\omega/c$.

1.3 Nonlinear optics

The linear dependence between polarization and electric field implies that the optical properties of matter such as refraction or absorption are constant quantities whose values are determined only by intrinsic features of the material and the optical frequency of the field. However, in the presence of high intensity irradiation provided by a laser light, the linear approximation doesn't hold anymore.

When the light intensity is sufficiently high, a small additional polarization term appears, so that the total polarization can be written as:

$$\tilde{\mathbf{P}} = \tilde{\mathbf{P}}_{\mathbf{L}} + \tilde{\mathbf{P}}_{\mathbf{NL}} \tag{1.12}$$

where $\tilde{\mathbf{P}}_{\mathbf{NL}}$ denotes the nonlinear part of the polarization.
Using the definition of polarization provided in Eq. 1.12, the propagation of the light inside the nonlinear medium is described by:

$$\nabla^2\tilde{\mathbf{E}} - \frac{1}{c^2}\frac{\partial^2}{\partial t^2}\tilde{\mathbf{E}} - \frac{1}{\epsilon_0 c^2}\frac{\partial^2}{\partial t^2}\tilde{\mathbf{P}}_{\mathbf{L}} = \frac{1}{\epsilon_0 c^2}\frac{\partial^2}{\partial t^2}\tilde{\mathbf{P}}_{\mathbf{NL}} \tag{1.13}$$

This relation has the form of a driven (i.e. inhomogeneous) wave equation where the nonlinear response of the medium acts as a source term which appears on the right -hand side of this equation. For a lossless and dispersionless medium this dependence is usually written in the following way:

$$\tilde{P}_i = \tilde{P}_{L(i)} + \epsilon_0 \sum_{jk} \chi_{ijk}^{(2)}\tilde{E}_j\tilde{E}_k + \epsilon_0 \sum_{jkl} \chi_{ijkl}^{(3)}\tilde{E}_j\tilde{E}_k\tilde{E}_l + ... = \tilde{P}_{L(i)} + \tilde{P}_i^{(2)} + \tilde{P}_i^{(3)} + ... \tag{1.14}$$

Here, the indices i, j, k, l refer to the Cartesian components of the field, $\chi^{(2)}_{ijk}$ and $\chi^{(3)}_{ijkl}$ are the third- and fourth-rank tensors of second- and third-order susceptibilities, respectively. Hence, $\tilde{\mathbf{P}}^{(\mathbf{2})}(\mathbf{r},t) = \epsilon_0\chi^{(2)} : \tilde{\mathbf{E}}^{(2)}(\mathbf{r},t)$ is the second-order polarization, $\tilde{\mathbf{P}}^{(\mathbf{3})}(\mathbf{r},t) = \epsilon_0\chi^{(3)} : \tilde{\mathbf{E}}^{(3)}(\mathbf{r},t)$ is the third-order polarization, and so on.

The occurrence of nonlinear interactions is also related to the symmetry of the nonlinear medium. For example, the second order effects (and all higher order effects with even order) are observed only in the non-centrosymmetric crystals, that is in crystals that do not display inversion symmetry. All elements of $\chi^{(\mathbf{2})}$ vanish in centrosymmetric media; on the other hand, $\chi^{(\mathbf{3})}$ has always non-zero elements in all type of media.

In general, all materials are lossy and dispersive: hence, the nonlinear optical susceptibilities become complex quantities. Moreover, if the electric vector of the optical field is composed by a few discrete frequency components, then the total induced polarization vector is given by:

$$\tilde{\mathbf{P}}(\mathbf{r},t) = \sum_m \mathbf{P}(\omega_m)\exp(-i\omega_m t) \tag{1.15}$$

where m denotes the number of frequencies involved. Here $\mathbf{P}(\omega_m) = \mathbf{P}(\mathbf{r},t)\exp(i\mathbf{k}_m\mathbf{r})$ is the complex amplitude assigned to the component with frequency ω_m.

1.4 Nonlinear index of refraction

Under the action of intense coherent light, the contribution of the nonlinear polarization to the refractive index can no longer be neglected. To introduce the phenomenon let us consider an isotropic medium ($\chi^{(2)} = 0$), where only the third-order effects are present and a linearly polarized plane wave of frequency ω is propagating in the z direction. Then the third order polarization is given by:

$$P^{(3)}(\omega) = 3\epsilon_0\chi^{(3)}(\omega;\omega,\omega-\omega)E(\omega)E(\omega)E^*(\omega) \tag{1.16}$$

where $E^*(\omega) = E(-\omega)$. For simplicity, vector and tensor indices are suppressed (e.g. here: $\chi^{(3)} = \chi^{(3)}_{xxxx}$). Hence the total polarization of the material system is described by Eq. 1.6+ Eq. 1.16:

$$P(\omega) = \epsilon_0\chi_{eff}E(\omega) \tag{1.17}$$

where $\chi_{eff} = \chi^{(1)} + 3\chi^{(3)}|E(\omega)|^2$ is the effective susceptibility. Assuming that the nonlinear contribution to χ_{eff} is much smaller than the linear one, the general expression for a refractive

index can be expressed as (see Appendix A.2 for calculations):

$$n = \sqrt{1 + Re\{\chi_{eff}\}} \approx n_0 + \frac{3}{2n_0}\chi_R^{(3)}|E(\omega)|^2 \tag{1.18}$$

Taking into account the time averaged intensity of the optical field, the nonlinear part of the refractive index is described by (see Appendix A.2 for calculations):

$$n_2 = \frac{3}{4n_0^2\epsilon_0 c}\chi_R^{(3)} \tag{1.19}$$

From Eqs. 1.18 and 1.19 it is clearly seen that for weak incident beams, the refractive index of a medium remains constant (independent of the incident light intensity) since the contribution of Δn is negligible. However, when the incident light is intense enough, the refractive is no more constant but depends noticeably of the incident optical wave.

1.5 Two-photon absorption

Nonlinear absorption effects are resonant phenomena which refer to the change in the transmittance of a material as a function of the intensity. Among this class of effects, we can generally distinguish excited state absorption (including saturable absorption and free-carrier absorption) or multi-photon absorption. The latter one is of particular importance because it often accompanies a change of the refraction due to non-resonant electronic response. At sufficiently high intensities, the probability of a material absorbing more than one photon before relaxing to the ground state is greatly enhanced. Particularly, the simultaneous transition of two photons is a very well-known and a frequently observed phenomenon.

In the most general case, two optical fields at frequencies ω and ω' are present, and one photon from each field is absorbed making an overall transition approximately at $\omega + \omega'$. If $\omega = \omega'$, the linear Lambert-Beer law is generalized in the following way:

$$\frac{dI}{dz} = -\alpha I - \beta I^2 \tag{1.20}$$

where β is the TPA coefficient (expressed in m/W in SI units). This quantity is directly related to the imaginary part of the third order susceptibility (see Appendix A.3 for calculations):

$$\beta = \frac{3\pi}{n_0^2\epsilon_0 c\lambda}\chi_I^{(3)}. \tag{1.21}$$

Chapter 2

Z-scan measurement theory

In order to correctly interpret the results obtained from the Z-scan technique and to optimize the setup, a comprehensive theory of the Z-scan setup must be taken into account. This chapter is dedicated to provide such knowledge.

2.1 Z-scan technique Overview

Using a single tightly focused Gaussian laser beam, as depicted in Fig. 2.1, we measure the transmittance of a nonlinear medium through a finite aperture in the far field as a function of the sample position z with respect to the focal plane. The following example will qualitatively elucidate how such a trace (Z-scan) is related to the nonlinear refraction of the sample.[1]

Assume, for instance, a material with a negative nonlinear refractive index and a thickness smaller than the diffraction length of the focused beam (a thin medium). This can be regarded as a thin diverging lens with intensity-dependent focal length. Starting the scan from a distance far away from the focus (negative z), the beam irradiance is low and negligible nonlinear refraction occurs; hence, the transmittance (D2/D1 in Fig. 2.1) remains relatively constant. As the sample is brought closer to focus, the beam irradiance increases, leading to self-lensing in the sample. A negative self-lensing prior to focus will tend to collimate the beam, causing a beam narrowing at the aperture which results in an increase in the measured transmittance. As the scan in z continues and the sample passes the focal plane to the right (positive z), the same self-defocusing increases the beam divergence, leading to beam broadening at the aperture, and thus a decrease in transmittance. This suggests that there is a null as the sample crosses the focal plane. This is analogous to placing a thin

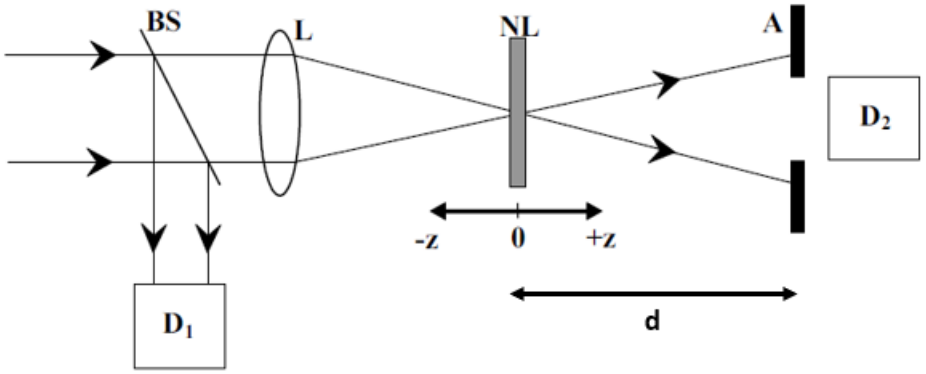

Figure 2.1: The Z-scan experimental apparatus in which the ratio D2/D1 is recorded as a function of the sample position z.[1]

lens at or near the focus, resulting in a minimal change of the far-field pattern of the beam. The Z-scan is completed as the sample is moved away from focus (positive z) such that the transmittance becomes linear since the irradiance is again low.

A prefocal transmittance maximum (peak) followed by the Z-scan is a signature of a negative refractive nonlinearity. Positive nonlinear refraction, following the same analogy, gives rise to an opposite valley-peak configuration, as shown in Fig. 2.2.
It is an extremely useful feature of the Z-scan method that the sign of the nonlinear index is immediately obvious from the data, and as we will show in the following section, the magnitude can also be easily estimated using a simple analysis for a thin medium.

In the above Z-scan picture, a purely refractive nonlinearity was considered, assuming that no absorptive nonlinearities (such as multiphoton absorption or absorption saturation) are present. Qualitatively, multiphoton absorption suppresses the peak and enhances the valley, while absorption saturation produces the opposite effect. The sensitivity to nonlinear refraction is entirely due to the aperture, and removal of the aperture completely eliminates the effect. The open aperture measurement yields the curve in Fig. 2.3.

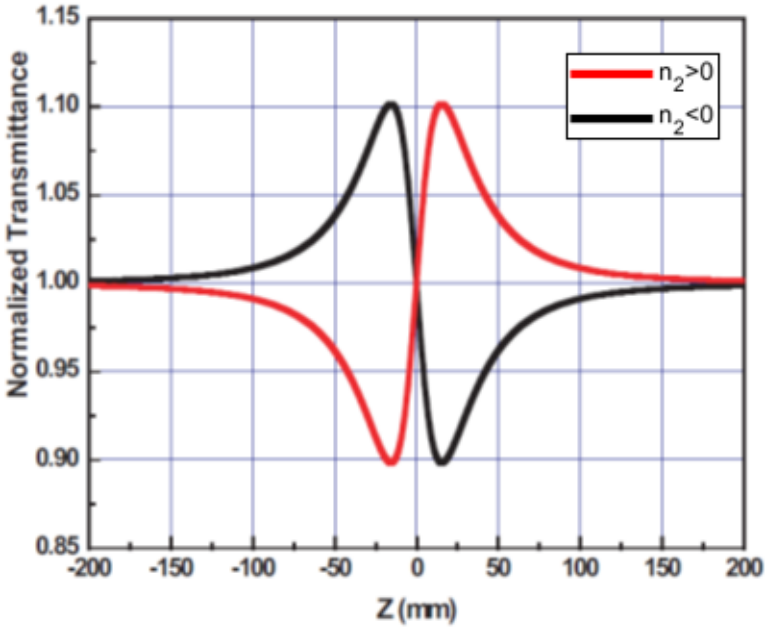

Figure 2.2: Example of nonlinear refraction in a z-scan experiment. The red curve corresponds to a positive phase shift (self-focusing) while the black curve corresponds to a negative phase shift (self-defocusing).[3]

2.2 Z-scan technique: pure nonlinear diffraction ($\beta = 0$) [1]

Recalling Section 1.1 for the notation, since we are concerned with calculating the radial phase variations $\delta\Phi(r)$, the slowly varying envelope approximation (SVEA) applies, and all other phase changes that are uniform in r are ignored.

If the sample thickness is so small that one can neglect changes in the beam diameter within the sample due to either diffraction or nonlinear refraction, the medium is regarded as "thin" and the self-refraction process is referred to as "external self-action" [4]. For linear diffraction, this implies that $L << z_0$, while for nonlinear refraction, $L << z_0/\Delta\Phi(0)$, where $\Delta\Phi(0) = k\Delta n_0 L$. In most Z-scan experiments, we find that the second criterion is automatically met since $\Delta\Phi(0)$ is small. Additionally, we have found that the first criterion for linear diffraction is too restrictive, and it is sufficient to replace it with $L < z_0$.

Such an assumption simplifies the problem considerably, and the amplitude and phase Φ of the electric field as a function of z' are now governed in the SVEA by a pair of simple equations:

$$\frac{d\Delta\Phi}{dz'} = \Delta n(I)k \tag{2.1}$$

$$\frac{dI}{dz'} = -\alpha(I)I \tag{2.2}$$

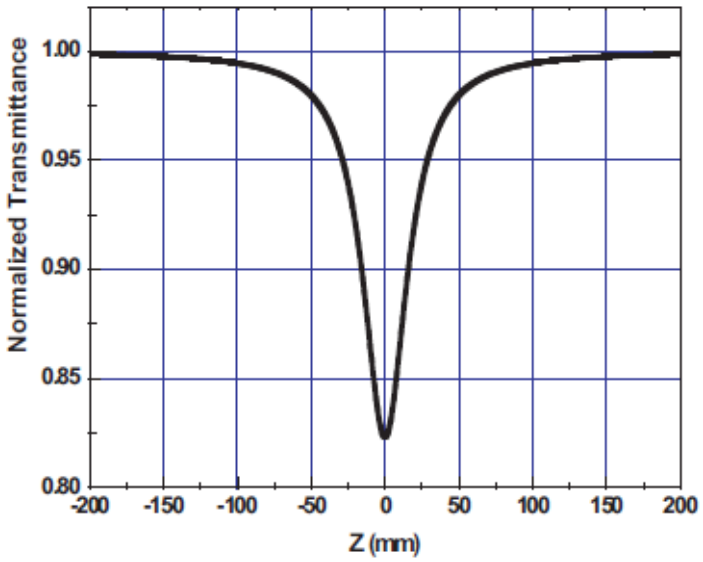

Figure 2.3: Example of nonlinear absorption in a z-scan experiment. The curve reveals an increase of the absorption of the material with an increase in the light intensity.[3]

where z' is the propagation depth in the sample and $\alpha(I)$, in general, includes linear and nonlinear absorption terms. Note that z' should not be confused with the sample position z. In the case of a cubic nonlinearity and negligible nonlinear absorption, Eqs. 2.1 and 2.2 are solved to give the phase shift $\Delta\Phi$ at the exit surface of the sample, which simply follows the radial variation of the incident irradiance at a given position of the sample z. Thus,

$$\Delta\Phi(z,r,t) = \Delta\Phi_0(z,t)\exp\left(-\frac{2r^2}{w^2(z)}\right) \tag{2.3}$$

with: $\Delta\Phi_0(z,t) = \frac{\Delta\Phi_0(t)}{1+z^2/z_0^2}$. $\Delta\Phi_0(t)$, the on-axis phase shift at the focus, is defined as

$$\Delta\Phi_0(t) = k\Delta n_0(t)L_{\text{eff}} \tag{2.4}$$

where $L_{\text{eff}} = (1-e^{-\alpha L})/\alpha$, with L the sample thickness and α the linear absorption coefficient. Here, $\Delta n_0(t) = n_2 I_0(t)$ with $I_0(t)$ being the on-axis irradiance at focus ($z = 0$).
In this case the complex electric field E_e exiting the sample, contains the nonlinear phase distortion:

$$E_e(r,z,t) = E(r,z,t)e^{-\alpha L/2}e^{i\Delta\Phi(r,z,t)}. \tag{2.5}$$

While in general the far-field pattern of the beam at the aperture plane is given by Huygen's principle, a more convenient treatment called the "Gaussian decomposition" (GD) method given by Weaire et al.[4] allows to perform the same kind of calculation more efficiently.

With this method, the complex electric field at the exit plane of the sample is decomposed into a sum of Gaussian beams through a Taylor series expansion of the nonlinear phase term $e^{i\Delta\Phi(r,z,t)}$ in Eq. 2.5:

$$e^{i\Delta\Phi(r,z,t)} = \sum_{m=0}^{\infty} \frac{[i\Delta\Phi_0(z,t)]^m}{m!} e^{-2mr^2/w^2(z)}. \tag{2.6}$$

Each Gaussian beam can now be simply propagated to the aperture plane where they will be re-summed to reconstruct the beam. When including the initial beam curvature for the focused beam, the resultant electric field pattern at the aperture can be derived as [4]:

$$E_a(r,t) = E(z, r=0, t)e^{-\alpha L/2} \sum_{m=0}^{\infty} \frac{[i\Delta\Phi_0(z,t)]^m}{m!} \frac{w_{m0}}{w_m} \exp\left(-\frac{r^2}{w_m^2} - \frac{ikr^2}{2R_m} + i\theta_m\right). \tag{2.7}$$

Defining d as the propagation distance in free space from the sample to the aperture plane and $g = 1 + d/R(z)$, the remaining parameters in Eq. 2.7 are expressed as:

$$w_{m0}^2 = \frac{w^2(z)}{2m+1}$$

$$d_m = \frac{kw_{m0}^2}{2}$$

$$w_m^2 = w_{m0}^2 \left[g^2 + \frac{d^2}{d_m^2}\right]$$

$$R_m = d\left[1 - \frac{g}{g^2 + d^2/d_m^2}\right]^{-1}$$

$$\theta_m = \tan^{-1}\left[\frac{d/d_m}{g}\right].$$

Eq. 2.7 is a general case derived by Weaire et al. [4] where they considered a collimated beam ($R = \infty$) for which $g = 1$. This Gaussian Decomposition (GD) method is very useful for the small phase distortion detected with the Z-scan method, since it requires only a few terms of the sum in Eq. 2.7.

The transmitted power through the aperture is obtained by spatially integrating $|E_a(r,t)|^2$ up to the aperture radius r_a, giving:

$$P_T(\Delta\Phi_0(t)) = c\epsilon_0 n_0 \pi \int_0^{r_a} |E_a(r,t)|^2 r dr \tag{2.8}$$

Including the pulse temporal variation, the normalized Z-scan transmittance $T(z)$ can be calculated as:

$$T(z) = \frac{\int_{-\infty}^{\infty} P_T(\Delta\Phi_0(t))dt}{S\int_{-\infty}^{\infty} P_i(t)dt} \tag{2.9}$$

where $P_i(t) = \pi w_0^2 I_0(t)/2$ is the instantaneous input power (within the sample) and $S = 1 - \exp(-2r_a^2/w_a^2)$ is the aperture linear transmittance, with w_a denoting the beam radius at the aperture in the linear regime.

First, let us consider an instantaneous nonlinearity and a temporally square pulse to illustrate the general features of the Z-scan. This is equivalent to assuming that radiation is Continuous Wave and the nonlinearity has reached the steady state. The normalized transmittances in the far field are shown in Fig. 2.4, for $\Delta\Phi_0 = \pm 0.25$ and a small aperture ($S = 0.01$).

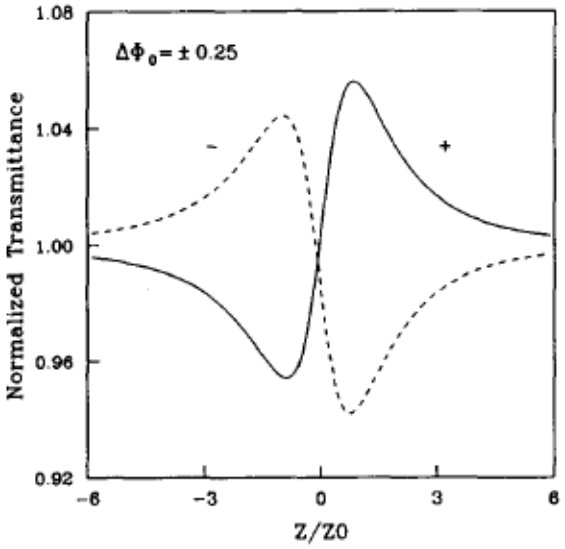

Figure 2.4: Calculated Z-scan transmittance curves for a cubic nonlinearity with either polarity and a small aperture ($S = 0.01$).

They exhibit the expected features, namely, a valley-peak ($v-p$) for the positive nonlinearity and a peak-valley ($p - v$) for the negative one. For a given $\Delta\Phi_0$, the magnitude and shape of $T(z)$ do not depend on the wavelength or geometry as long as the far-field condition for the aperture plane ($d >> z_0$) is satisfied. The aperture size S, however, is an important parameter since a large aperture reduces the variations in $T(z)$. This reduction is more prominent in the peak where beam narrowing occurs and can result in a peak transmittance which cannot exceed $(1-S)$. Needless to say, for very large aperture or no aperture ($S = 1$), the effect vanishes and $T(z) = 1$ for all z and $\Delta\Phi_0$. An easily measurable quantity, ΔT_{p-v} can be defined as the difference between the normalized peak and valley transmittance:

$T_p - T_v$. In order to derive the relation between ΔT_{p-v} and $\Delta\Phi_0$, let us first assume that the on-axis electric field at the aperture plane can be obtained by letting $r = 0$ in Eq. 2.7. Furthermore, in the limit of small nonlinear phase change ($|\Delta\Phi_0| << 1$)), only two terms of the sum in Eq. 2.7 need be retained. Following such simplifications, the normalized Z-scan transmittance can be written as:

$$T(z, \Delta\Phi_0) = \frac{|E_a(z, r = 0, \Delta\Phi_0)|^2}{|E_a(z, r = 0, \Delta\Phi_0 = 0)|^2} = \frac{|(g + id/d_0)^{-1} + i\Delta\Phi_0(g + id/d_1)^{-1}|^2}{|(g + id/d_0)^{-1}|^2} \tag{2.10}$$

The far-field condition $d >> z_0$ can be used to further simplify Eq. 2.10 to give a geometry-independent normalized transmittance as:

$$T(z, \Delta\Phi_0) \approx 1 - \frac{4\Delta\Phi_0 x}{(x^2 + 9)(x^2 + 1)} \tag{2.11}$$

where $x = z/z_0$. The extrema (peak and valley) of the Z-scan transmittance can be calculated by solving the equation $dT(z, \Delta\Phi_0)/dz = 0$. Solutions to this equation yield:

$$x_{p,v} = \pm\sqrt{\frac{\sqrt{52} - 5}{3}} \approx \pm 0.858. \tag{2.12}$$

Therefore, the peak-valley separation can be written as:

$$\Delta Z_{p-v} \approx 1.7 z_0 \tag{2.13}$$

Also, inserting the x values from Eq. 2.12 into Eq. 2.11, the peak-valley transmittance change is:

$$\Delta T_{p-v} = \frac{8|x_{p,v}|}{(x_{p,v}^2 + 9)(x_{p,v}^2 + 1)}\Delta\Phi_0 = 0.406\Delta\Phi_0. \tag{2.14}$$

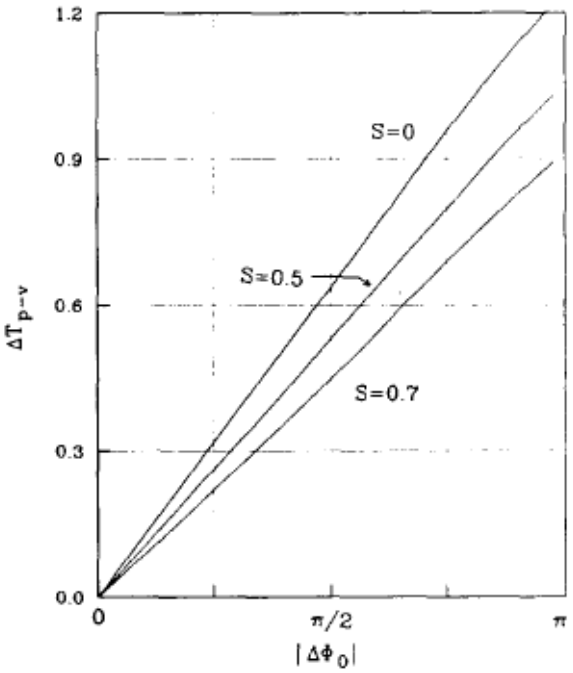

Figure 2.5: Calculated ΔT_{p-v}, as a function of the phase shift at the focus $|\Delta\Phi_0|$. The sensitivity, as indicated by the slope of the curves, decreases slowly for larger aperture sizes ($S > 0$).

Numerical calculations performed by Sheik-Bahae in [1] show that this relation is accurate to within 0.5% for $|\Delta\Phi_0| \leq \pi$. As shown in Fig. 2.5, for larger apertures, the linear coefficient 0.406 decreases to about 0.34 for $S = 0.5$,and about 0.29 for $S = 0.7$. Based on a numerical fitting, the following relationship can be used to include such variations within $\pm 2\%$ accuracy:

$$\Delta T_{p-v} \approx 0.406(1 - S)^{0.25}|\Delta\Phi_0|, \text{ for } |\Delta\Phi_0| \leq \pi. \tag{2.15}$$

2.3 Z-scan technique: nonlinear absorption ($\beta \neq 0$) [1]

In the presence of nonlinear absorption, the closed-aperture characteristic of Fig. 2.2 can no longer be obtained and one finds instead the curve of Fig. 2.6.

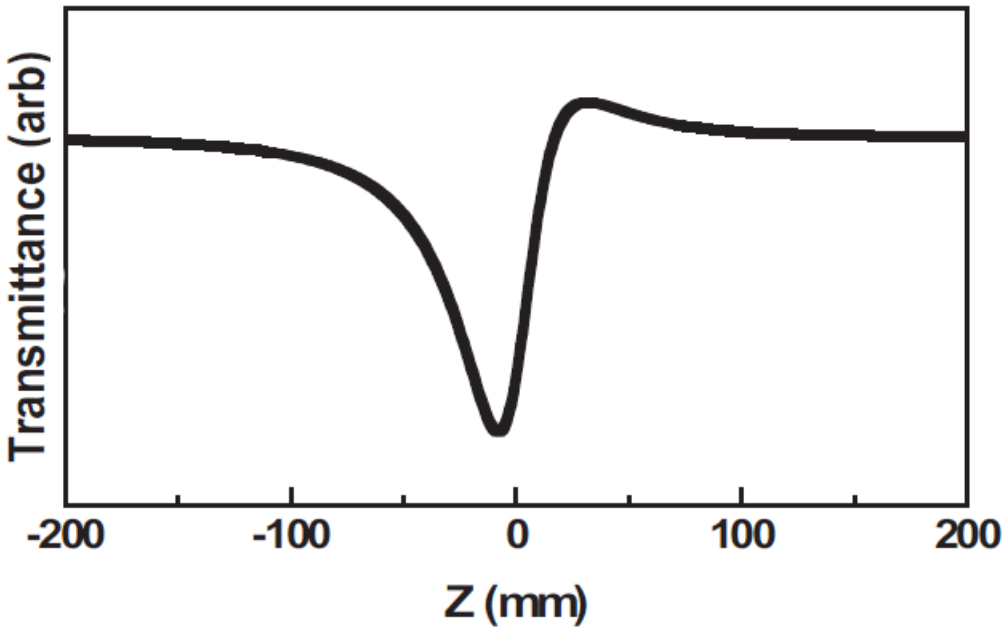

Figure 2.6: Closed-aperture scan in the presence of both nonlinear refraction and nonlinear absorption.

Even with nonlinear absorption, a Z-scan with a fully open aperture (S = 1) is insensitive to nonlinear refraction (thin sample approximation). Such Z-scan traces with no aperture are expected to be symmetric with respect to the focus (z = 0), where they have a minimum transmittance (e.g., multiphoton absorption, showed in Fig. 2.3) or maximum transmittance (e.g., saturation of absorption). In fact, the coefficients of nonlinear absorption can be easily calculated from such transmittance curves. By considering only two-photon absorption processes (for which $E_g/2 < \hbar\omega < E_g$) and recalling the relations used in Sections 1.4 and 1.5, this yields the irradiance distribution and phase shift of the beam at the exit surface of the sample as:

$$I_e(z,r,t) = \frac{I(z,r,t)e^{-\alpha L}}{1+q(z,r,t)} \tag{2.16}$$

and:

$$\Delta\Phi(z,r,t) = \frac{kn_2}{\beta}\ln[1+q(z,r,t)] \tag{2.17}$$

where $q(z,r,t) = \beta I(z,r,t)L_{\text{eff}}$ (again, z is the sample position).
Combining Eqs. 2.16 and 2.17, the following complex electric field at the exit surface of the

sample is obtained:

$$E_e = E(z,r,t)e^{-\alpha L/2}[1+q(z,r,t)]^{(ikn_2/\beta-1/2)} \tag{2.18}$$

Eq. 2.18 reduces to Eq. 2.5 in the limit of no two-photon absorption. For $|q|<1$, following a binomial series expansion in powers of q, Eq. 2.18 can be expressed as an infinite sum of Gaussian beams similar to the purely refractive case:

$$E_e = E(z,r,t)e^{-\alpha L/2}\sum_{m=0}^{\infty}\frac{q(z,r,t)^m}{m!}\prod_{n=0}(ikn_2/\beta-1/2-n+1) \tag{2.19}$$

where the Gaussian spatial profiles are implicit in $q(z,r,t)$ and $E(z,r,t)$. The complex field pattern on the aperture plane can be obtained in the same manner as before. The result can again be represented by Eq. 2.7 if we substitute the $[i\Delta\Phi_0(z,t))]^m/m!$ terms in the sum by:

$$f_m = \frac{[i\Delta\Phi_0(z,t)]^m}{m!}\prod_{n=0}^{m}\left[1+i(2n-1)\frac{\beta}{2kn_2}\right] \tag{2.20}$$

with $f_0 = 1$.

The Z-scan transmittance variations can be calculated following the previous procedure. As is evident from Eq. 2.20, the absorptive and refractive contributions to the far-field beam profile, and hence to the Z-scan transmittance, are coupled. When the aperture is removed, however, the Z-scan transmittance is insensitive to beam distortion and is only a function of the nonlinear absorption. In that case ($S=1$) the total transmitted fluence can be obtained by spatially integrating Eq. 2.16 without having to include the free-space propagation process. Integrating Eq. 2.16 over r at z, we obtain the transmitted power $P(z,t)$:

$$P(z,t) = P_i(t)e^{-\alpha L}\frac{\ln[1+q_0(z,t)]}{q_0(z,t)} \tag{2.21}$$

with $q_0(z,t) = \beta I_0(t)L_{eff}/(1+z^2/z_0^2)$ and $P_i(t)$ defined in Eq. 2.9. For a temporally Gaussian pulse, Eq. 2.21 can be time integrated to give the normalized energy transmittance:

$$T(z,S=1) = \frac{1}{\sqrt{\pi q_0(z,0)}}\int_{-\infty}^{\infty}\ln[1+q_0(z,0)e^{-t^2}]dt \tag{2.22}$$

For $|q_0| < 1$, this transmittance can be expressed in terms of the peak irradiance in a summation form more suitable for numerical evaluation [1]:

$$T(z, S = 1) = \sum_{m=0}^{\infty} \frac{[-q_0(z, 0)]^m}{(m + 1)^{3/2}} \qquad (2.23)$$

Thus, once an open-aperture ($S = 1$) Z-scan is performed, the nonlinear absorption coefficient β can be unambiguously deduced. With β known, the Z-scan with aperture in place ($S < 1$) can be used to extract the remaining unknown, namely, the coefficient n_2.

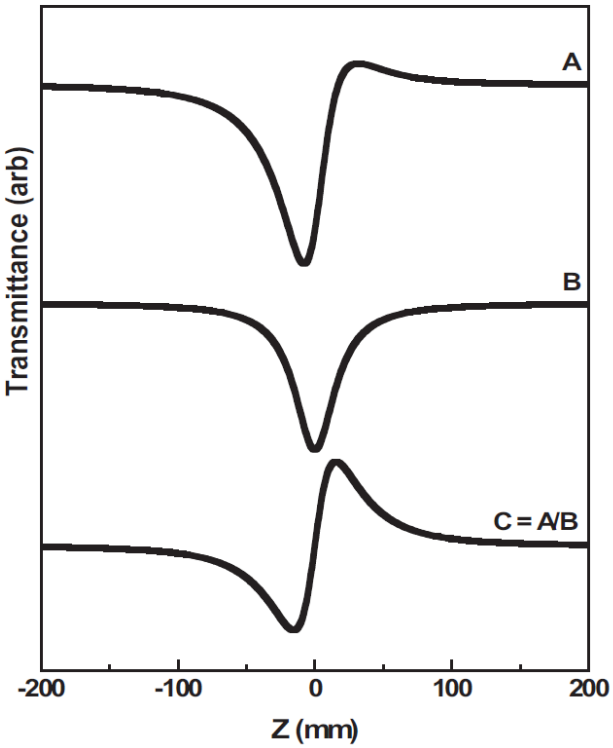

Figure 2.7: Simulated z-scan signal in the presence of both nonlinear refraction and nonlinear absorption. The top curve (A) is the result of the closed aperture scan. The middle curve (B) is the result of the open aperture scan. The bottom curve (C) estimates the closed aperture result in the absence of NLA, and is obtained by dividing the actual closed aperture measurement (A) by the open aperture measurement (B).

As was done in the case of a purely refractive effect, it is desirable to estimate n_2 and β without having to perform a detailed fitting of the experimental data. The separation and evaluation process of n_2 is simple: divide the closed aperture ($S < 1$) normalized Z-scan (with background subtracted) by the one with open aperture ($S = 1$). The result is a new Z-scan where ΔT_{p-v} agrees to within $\pm 10\%$ of that obtained from a purely refractive Z-scan. This procedure is shown in Fig. 2.7. A thorough numerical evaluation of the theoretical results obtained by Sheik-Bahae [1] indicates that within less than 10% uncertainty, such a procedure is possible provided that $q_0(0, 0) \leq 1$ and $\beta/2kn_2 \leq 1$. The first condition can be met by adjusting the irradiance. The second condition is an intrinsic property of the material implying that the $Im(\chi^{(3)})$ should not be larger than the $Re(\chi^{(3)})$.

Chapter 3

Z-scan setup: optimization and calibration

In this chapter, I will outline the role of relevant parameters in the optimization of the measurements, along with the description of my setup and a comprehensive list of the components used.

3.1 Critical parameters

For the Z-scan setup to work correctly, let us recall again the conditions that must be satisfied:

- a Gaussian impinging beam;
- $z_0 >> L$, with L the sample thickness and z_0 the Rayleigh range;
- $z_0 >> L\Delta\Phi(0)$, with $\Delta\Phi(0)$ the induced phase variation when the sample is placed in the focus.

Hence, the sample thickness acts as the bottleneck of our setup. Another critical parameter is the beam waist w_0 (see Section 1.1): a small w_0 ensures a high peak intensity $\hat{I}$ on the sample in the focus, as in a pulsed laser these two quantities are related by the following formula:

$$\hat{I} = \frac{\overline{P}}{f_{rep}\tau A} \tag{3.1}$$

where $\overline{P}$ represents the time-averaged power of the laser (easily measured with a high-power photodiode), f_{rep} is the repetition rate of the laser, τ the pulse width, and $A = \pi w_0^2$ the area

where the maximum power of the Gaussian beam is concentrated. However, z_0 and w_0 are not independent quantities as $z_0 = \frac{\pi}{\lambda} w_0^2$. Luckily, w_0 can be easily controlled by choosing a lens with a suitable focal distance. Assuming that the beam impinging of the focusing lens is perfectly collimated, w_0 and the incident beam diameter D are related via the following equation [5]:

$$w_0 = \frac{2\lambda}{\pi} \frac{f}{D} \tag{3.2}$$

This formula also shows the dependence of w_0 on λ of the setup. Fig. 3.1, reports the calculated values of w_0 and z_0 as a function of λ, for an incident beam diameter of ≈ 3.5 mm (a rough estimate of the laser beam after the collimation step, done with a fluorescent card) and different values of the focal distance of the focusing lens. By doing so, the optimal choice for the focusing lens is $f = 20$ cm, as it allows to satisfy the condition $z_0 > L$ for a very large band ($\lambda \in [1000, 1500]$ nm).

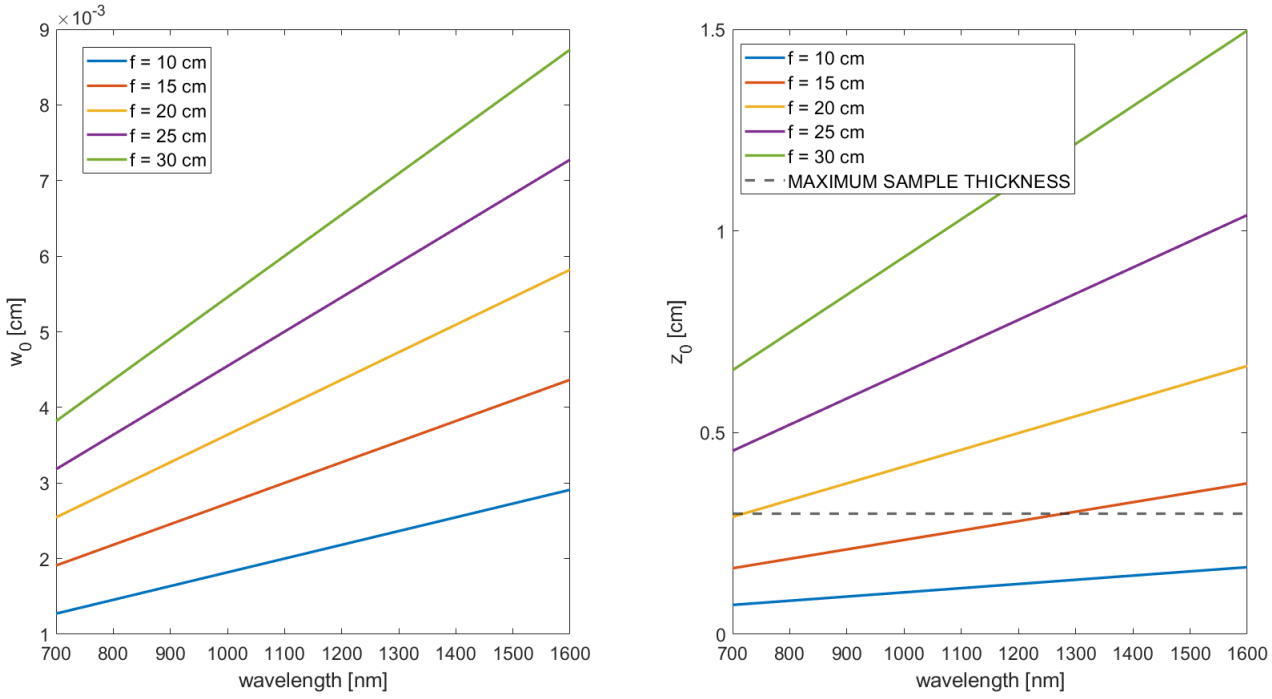

Figure 3.1: Calculated waist and Rayleigh range vs. wavelength for different focal distances f. The black line represents the maximum thickness of our samples (2 mm).

3.2 Final setup

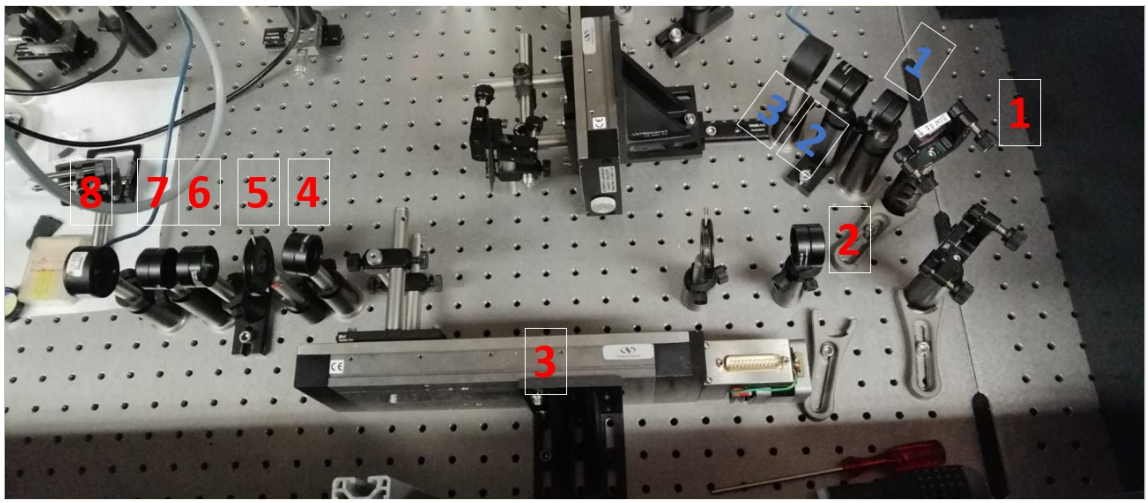

Figure 3.2: My final Z-scan setup. The red numbers mark the components on the main arm of the setup; the blue numbers mark the components of the reference arm.

My Z-scan setup includes two parts: the main arm, on which the sample is placed, and the reference arm, responsible for checking the laser stability. The main arm (red numbers in Fig. 3.2) hosts the following components:

1) BSN11 (a 90/10 beam-splitter)

2) LA1708-B (f = 200 mm lens)

3) M-UTM150PP1HL (motorized stage)

4) NE60AB (optical density)

5) ID25 (aperture)

6) LA1608-C-ML (f = 75 mm lens)

7) NE30AB (optical density)

8) 818IG (InGaAs photodiode)

The reference arm (blue numbers in Fig. 3.2) hosts the following components:

1) NE40AB (optical density)

2) LB1761-B (f = 25.4 mm lens)

3) 818IR (Ge photodiode)

Other components that do not appear in Fig. 3.2 are:

- MM4006 (motion controller)
- power meter
- SATSUMA (Femtosecond fiber laser)
- MANGO (OPA, see Appendix B for more information)

3.3 Knife-edge technique

In order to have a precise estimation of n_2, a sound characterization of the TEM_{00} Gaussian beam profile is needed. To this end, we resort to a measurement of the beam waist via the knife-edge technique [6]. As shown in Fig. 3.3, this is performed by placing a sharp blade on the path of the laser beam and a photodiode after it. As the blade is translated along x, the photodiode measures the power of the portion of the beam that is not shielded by the blade.

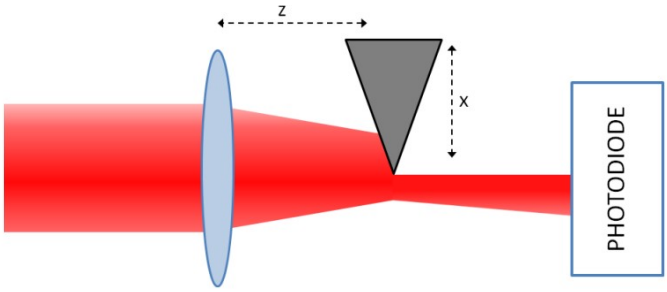

Figure 3.3: Knife-edge technique schematic.

Combining Eq. 1.1 and $I = 2nc\epsilon_0|E|^2$, where I is the intensity profile of a Gaussian beam, we get [6]:

$$I(x,y) = I_0 \exp\left(-2\frac{(x+y)^2}{w_0^2}\right) \tag{3.3}$$

As the blade moves along x, the power measured by the photodiode varies in the following way:

$$P(x) = \int_x^{+\infty}\int_{-\infty}^{+\infty} I(x,y)dxdy = P_0\frac{1}{2}\left[1 - \text{erf}\left(\sqrt{2}\frac{x-x_0}{w_0}\right)\right] = P_0\frac{1}{2}\text{erfc}\left(\sqrt{2}\frac{x-x_0}{w_0}\right) \tag{3.4}$$

By interpolating $P(x)$ with the above expression, w_0 can be easily retrieved. In order to simplify the fitting process, I normalized all the measurements with respect to the maximum

power value. In Fig. 3.4, I show the knife-edge measurement of the unfocused beam. The measured power profile is well fitted with $w_0 = 2.8$ mm, which is not too different from the value used in Section 3.1. In Fig. 3.5, I show the knife-edge measurement performed in the beam focus. While the curve looks rough when compared to the one reported in Fig. 3.4 (mainly due to the finite sharpness of the blade), I was yet able to extract the following value: $w_0 = 33$ μm. Since Eq. 3.2 provides $w_0 = 32$ μm, the value found by me is very close to the theoretical one.

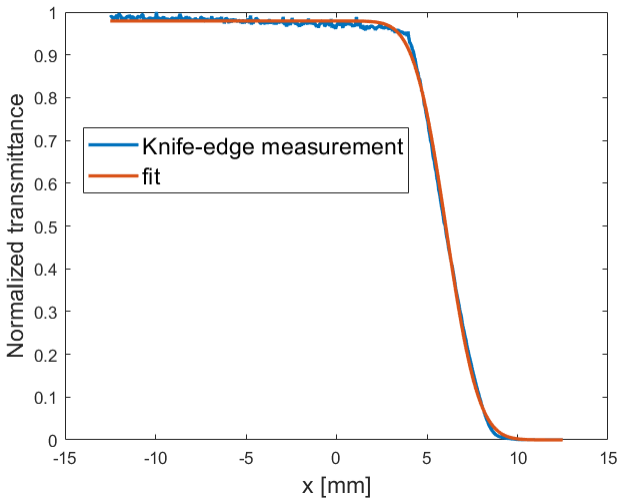

Figure 3.4: Knife-edge measurement of the unfocused beam.

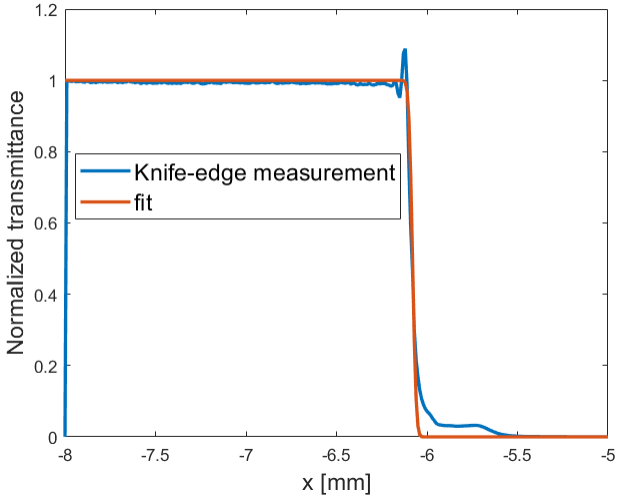

Figure 3.5: Knife-edge measurement of the focused beam.

Chapter 4

Calibration measurements

In order to check the correct functionality of my Z-scan setup, I performed a series of measurements on three different samples:

- NG11 sample (2 mm thick)
- a piece of microscope glass (1 mm thick)
- a polished GaAs sample (350 μm thick)

These samples have been chosen due to the possibility to compare the results with a variety of literature references. All measurements have been performed at
$\lambda = 1000$ nm.

4.1 Analysis of the glass samples

First, to check the sensitivity of the sample, the NG11 and the microscope glass sample have been studied. Due to the very weak nonlinearity of glasses ($n_2 \approx 10^{-20}$ m^2/W [7]), the measurement have been performed at the maximum power available: $\bar{P} = 130$ mW. The Z-scan characteristic curve is clearly seen in both Fig. (4.1A) and Fig. (4.1B). It is interesting to notice that, even at this high power, there is little to no nonlinear absorption: Fig. (4.1A) shows a clear flat signal when the aperture is fully open. It is also interesting to appreciate the difference between the two signals: the NG11 gives rise to a ΔT_{p-v} of almost 9% of the normalized transmittance, while the ΔT_{p-v} of the microscope glass is not larger than 2% of the normalized transmittance. Since only one measurement has been performed on the NG11 sample, it was assigned to it the theoretical relative error of $\pm 2\%$, found in Section 2.2. For the microscope glass, an absolute error of $\pm 0.1 \cdot 10^{-20}$ m^2/W was obtained

from the measurements. In the table below are reported the values of n_2, evaluated via Eq.

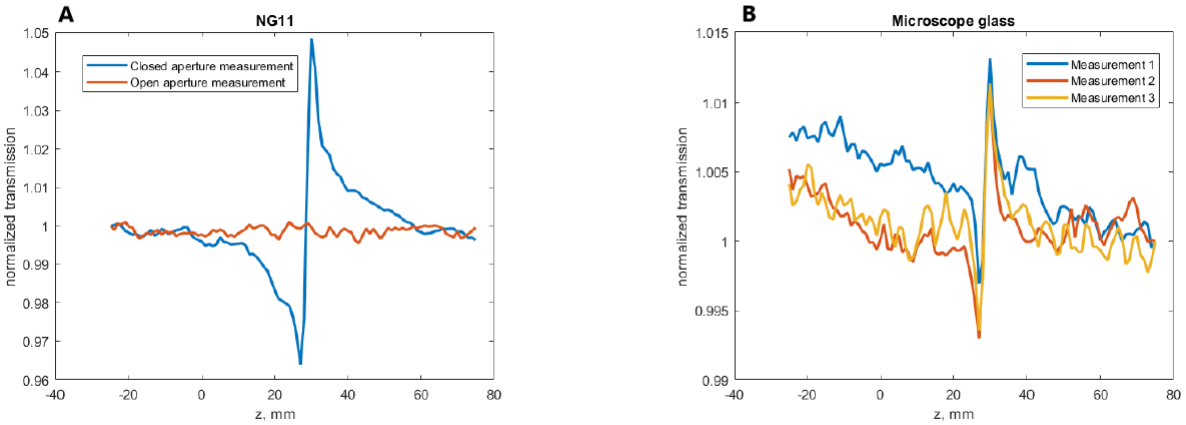

Figure 4.1: (A): Z-scan characteristic of the NG11 sample with both open and closed aperture. (B): 3 consecutive measurements of the microscope glass sample, with closed aperture.

2.15.

Table 4.1: n_2 values for glasses

Sample	n_2 [m^2/W]
NG11	$(5.42\pm0.1)\cdot10^{-20}$
Microscope glass (meas. 1)	$(1.04\pm0.1)\cdot10^{-20}$
Microscope glass (meas. 2)	$(1.17\pm0.1)\cdot10^{-20}$
Microscope glass (meas. 3)	$(1.14\pm0.1)\cdot10^{-20}$

4.2 Analysis of the GaAs sample

Unlike glass samples, GaAs is expected to provide much stronger nonlinear responses. For this reason, the power has been lowered significantly, in order to avoid the case for which $q_0 \geq 1$ (see Section 2.3 for more details). Two measurements have been performed: one at $\overline{P} = 7$ mW (Fig. 4.2), both with open and closed aperture, and one at $\overline{P} = 2$ mW (Fig. 4.3), also both with open and closed aperture. It is interesting to notice an important trade-off of the Z-scan characteristic: for low intensities, the characteristic becomes less defined, but, when nonlinear absorption is present, high intensities result in a heavily distorted curve. Hence, some trials are needed to determine the optimal power for a given measurement. For the open aperture measurements, this problem does not exist, as the characteristic is always well defined. Interestingly enough, at $\lambda = 1000$ nm, $n_2 < 0$. In the table below, are reported the values of n_2 and β for the two different powers and for the literature. The values are quite close.

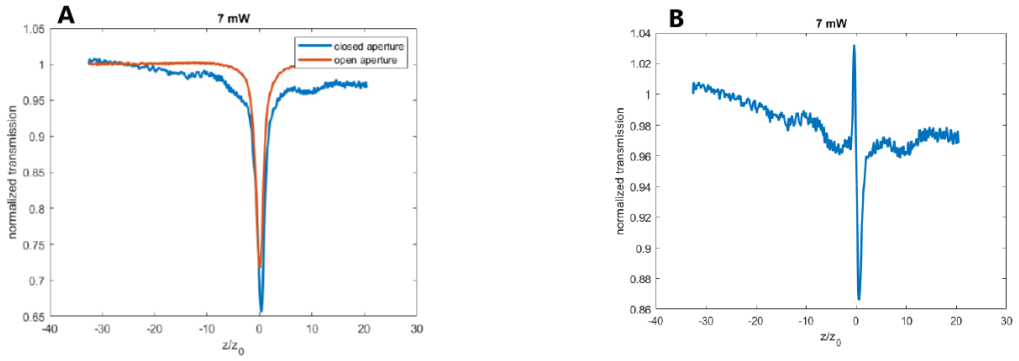

Figure 4.2: (A): Z-scan characteristic of the GaAs sample with both open and closed aperture at $P_{AVG} = 7$ mW. (B): ratio of the closed- to the open-aperture characteristic at $P_{AVG} = 7$ mW.

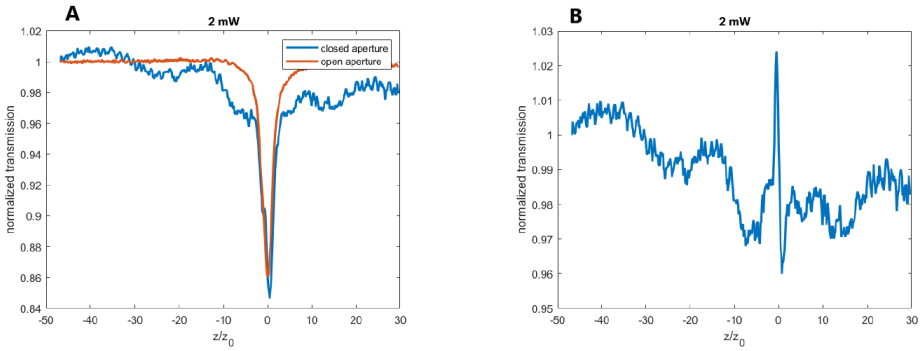

Figure 4.3: (A): Z-scan characteristic of the GaAs sample with both open and closed aperture at $\bar{P} = 2$ mW. (B): ratio of the closed- to the open-aperture characteristic at $\bar{P} = 2$ mW.

Table 4.2: n_2, β values for GaAs

$\bar{P}$ $[mW]$	n_2 [m^2/W]	β [m/W]
NG11	-1.06 · 10^{-20}	1.60 · 10^{-10}
7	-1.13 · 10^{-17}	1.30 · 10^{-10}
literature	-1.59 · 10^{-17} [8]	1.51 · 10^{-10} [9]

Conclusion

The Z-scan setup provides a simple, yet accurate way to characterize both n_2 and β in nonlinear materials. Thus, it becomes an important tool for what concerns nonlinear materials characterization.
For this reason, a collaboration with Alexandre Baron from Centre de Recherche Paul Pascal is under way: my Z-scan setup will be used to characterize the nonlinear optical response of a series colloidal plasmonic clusters. In particular, the four samples that will be analyzed are:

- a sample containing PANI dissolved in THF
- a sample containing PANI dissolved in ethanol
- a sample containing Ag nanoparticles suspended in ethanol
- a sample containing Ag/PANI core-shells in ethanol

where PANI stands polyaniline (a polymer) and THF for tetrahydrofuran (a solvent).
Thanks to the local field enhancement provided by the plasmonic Ag nanoparticles, the nonlinear response of PANI should be greatly enhanced; this enhancement should be measurable with my Z-scan setup.
The enhancing effect of these nanoparticles could then be used to enhance the nonlinear response of nonlinear metasurfaces.

Bibliography

[1] M. Sheik-Bahae, "Sensitive measurement of optical nonlinearities using a single beam," *IEEE Quantum Electronics*, vol. 26, pp. 760–769, 1990.

[2] K. Fedus, "Development of methods for measuring optical nonlinearities of third order," Ph.D. dissertation, Université d'Angers, 2011.

[3] "Application note: Z-scan for the characterization of transparent optical materials", technology and applications center, newport corporation," 2007.

[4] D. Weaire, "Effect of low-power nonlinear refraction on laser beam propagation in insb," *Opt. Lett.*, vol. 4, pp. 331–333, 1974.

[5] H. Yu, "Performance characterization of a miniaturized exploding foil initiator via modified visar interferometer and shock wave analysis," *Journal of Applied Physics*, vol. 121, no. 215901, pp. 1–10, 2017.

[6] M. M. Rashad, "Measurements of laser beam using knife edge technique," Ph.D. dissertation, Politecnico di Milano, 2011.

[7] J. Cimek, "Experimental investigation of the nonlinear refractive index of various soft glasses dedicated for development of nonlinear photonic crystal fibers," *OPTICAL Materials Express*, vol. 7, no. 10, pp. 3471–3483, 2017.

[8] M. Dinu, "Third-order nonlinearities in silicon at telecom wavelengths," *Appl. Phys. Lett.*, vol. 82, no. 18, pp. 2953–2956, 2003.

[9] W. Hurlbut, "Multiphoton absorption and nonlinear refraction of gaas in the mid-infrared," *Optics Letters*, vol. 32, no. 6, pp. 668–670, 2007.

Appendix A

Derivation of relevant formulas

A.1 Derivation of 1.8

Starting from the Helmotz equation:

$$\nabla^2 \mathbf{E}(\mathbf{r},\omega) - \epsilon_r \frac{\omega^2}{c^2}\mathbf{E}(\mathbf{r},\omega) = 0 \tag{A.1}$$

and recalling that $\epsilon_r = 1 + \chi^{(1)}$, with $\chi^{(1)} = \chi_R^{(1)} + i\chi_I^{(1)}$, if we assume a plane wave solution: $\mathbf{E}(\mathbf{r},\omega) = \mathbf{E}_0 \exp(i[kr - \omega t])$, the Helmotz equation reduces to:

$$k^2 = \epsilon_r \frac{\omega^2}{c^2} \tag{A.2}$$

Taking the square root on both sides:

$$K = \sqrt{\epsilon_r}\frac{\omega}{c} = \sqrt{1 + \chi_R^{(1)} + i\chi_I^{(1)}}\frac{\omega}{c} \tag{A.3}$$

Assuming $\chi_R^{(1)}(\omega) >> \chi_I^{(1)}(\omega)$, we can expand the square root:

$$\sqrt{1 + \chi_R^{(1)} + i\chi_I^{(1)}} = \sqrt{1 + \chi_R^{(1)}}\sqrt{1 + i\frac{\chi_I^{(1)}}{1 + \chi_R^{(1)}}} \approx \sqrt{1 + \chi_R^{(1)}}\left(1 + i\frac{\chi_I^{(1)}}{2(1 + \chi_R^{(1)})}\right)$$

Since $n_0 = \sqrt{1+\chi_R^{(1)}}$:

$$\sqrt{1+\chi_R^{(1)}+i\chi_I^{(1)}} \approx n_0\left(1+i\frac{\chi_I^{(1)}}{2n_0^2}\right) = n_0 + i\frac{1}{2n_0}\chi_I^{(1)}$$

Substituting back in Eq. A.3:

$$k = n_0\frac{\omega}{c} + i\frac{\omega}{2n_0 c}\chi_I^{(1)} \tag{A.4}$$

Usually, k is expressed as: $k = k' + i\frac{1}{2}\alpha$. Hence:

$$k' = n_0\frac{\omega}{c} \tag{A.5}$$

$$\alpha = \frac{\omega}{n_0 c}\chi_I^{(1)} \tag{A.6}$$

A.2 Derivation of 1.18 and 1.19

Defining $\chi_{\text{eff}} = \chi^{(1)} + 3\chi^{(3)}|E(\omega)|^2$ and $\epsilon_r = 1+\chi_{\text{eff}}$, the refractive index becomes:

$$n = \sqrt{\epsilon_r} = \sqrt{1+\chi_{\text{eff}}} = \sqrt{1+\chi^{(1)}+3\chi^{(3)}|E(\omega)|^2} \tag{A.7}$$

Assuming $\chi^{(3)} << \chi^{(1)}$, we can expand Eq. A.7:

$$\sqrt{1+\chi^{(1)}+3\chi^{(3)}|E(\omega)|^2} = \sqrt{1+\chi^{(1)}}\sqrt{1+\frac{3\chi^{(3)}|E(\omega)|^2}{1+\chi^{(1)}}} \approx \sqrt{1+\chi^{(1)}}\left(1+\frac{3\chi^{(3)}|E(\omega)|^2}{2(1+\chi^{(1)})}\right)$$

But $n_0 = \sqrt{1+\chi^{(1)}}$:

$$n \approx n_0 + \frac{3}{2n_0}\chi^{(3)}|E(\omega)|^2 \tag{A.8}$$

When the optical Kerr effect is present, n can be rewritten as:

$$n = n_0 + n_2 I \tag{A.9}$$

Recalling that:

$$I = 2c\epsilon_0 n_0|E|^2 \tag{A.10}$$

Eq. A.10 becomes:

$$n = n_0 + 2c\epsilon_0 n_0 n_2 |E|^2 \tag{A.11}$$

Since Eqs. A.8 and A.11 must be equal:

$$2c\epsilon_0 n_0 n_2 |E|^2 = \frac{3}{2n_0}\chi^{(3)}|E(\omega)|^2 n_2 = \frac{3}{4n_0^2 c\epsilon_0}\chi^{(3)}$$

A.3 Derivation of 1.21

Defining $\chi_{I,\text{eff}} = \chi_I^{(1)} + 3\chi_I^{(3)}|E(\omega)|^2$, α becomes:

$$\alpha = \frac{\omega}{n_0 c}\chi_I^{(1)} + \frac{3\omega}{n_0 c}\chi_I^{(3)}|E|^2 \tag{A.12}$$

When the optical Kerr effect is present, α can be rewritten as:

$$\alpha = \alpha_0 + \beta I \tag{A.13}$$

With $\alpha_0 = \frac{\omega}{n_0 c}\chi_I^{(1)}$. Recalling that:

$$I = 2c\epsilon_0 n_0 |E|^2 \tag{A.14}$$

Eq. A.13 becomes:

$$\alpha = \alpha_0 + 2c\epsilon_0 n_0 \beta |E|^2 \tag{A.15}$$

But, Eqs. A.12 and A.15 must be equal:

$$2c\epsilon_0 n_0 \beta = \frac{3\omega}{n_0 c}\chi_I^{(3)} \tag{A.16}$$

Hence:

$$\beta = \frac{3\omega}{2c^2\epsilon_0 n_0^2}\chi_I^{(3)} = \frac{3\pi}{2c\epsilon_0 n_0^2 \lambda}\chi_I^{(3)} \tag{A.17}$$

Appendix B

OPA Mango

All measurements in this report have been performed with a Mango OPA from Amplitude. An OPA (Optical Parametric Amplifier) allows for an easy and versatile frequency conversion for a pulsed laser. Optical parametric amplification is the physical process behind the frequency conversion; the process is shown in Fig. B.1.

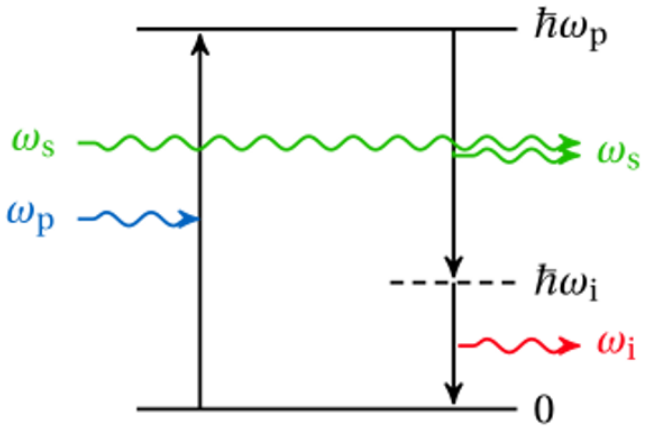

Figure B.1: Optical parametric amplification process.

Optical parametric amplification is a stimulated process: a pump photon $\hbar\omega_p$ is broken into two photons: a signal ($\hbar\omega_s$) and an idler ($\hbar\omega_i$). $\hbar\omega_s$ stimulates the process; due to energy conservation: $\hbar\omega_p = \hbar\omega_s + \hbar\omega_i$. The mango OPA characteristic are the following:

Table B.1: OPA Mango characteristics

Signal tuning range	630 - 1020 nm
Idler tuning range	1040 – 2600 nm
SHG signal	315 - 510 nm
FHG signal	210 - 255 nm
SHG idler	520 – 630 nm
FHG idler	260 – 315 nm
DFG	2600 – 11000 nm
Pulse duration	$<$ 300 fs
Repetition rate	Up to 1 MHz
Conversion efficiency	$>$12% at peak (signal + idler)
Bandwidth in cm^{-1}	70 –120 cm^{-1}
Polarization	Horizontal
Beam quality	TEM_{00}